# 25-Gb/s Direct Modulation of Implant Confined Holey Vertical-Cavity Surface-Emitting Lasers

Chen Chen, *Student Member, IEEE*, Zhaobing Tian, *Student Member, IEEE*, Kent D. Choquette, *Fellow, IEEE*, and David V. Plant, *Fellow, IEEE*

***Abstract*—A 25-Gb/s direct modulation of an 850-nm implant-confined holey vertical-cavity surface-emitting laser (VCSEL) is demonstrated with a low operation current density of 7.4 KA/cm$^2$. The high-speed performance arises from cavity designs that are achieved using standard fabrication and epitaxial materials. The etched holey structure is incorporated into the top mirror of the VCSEL to tailor the size of the optical cavity independent from that of the electrical current aperture, enabling us to achieve high-speed modulation and low operation current density simultaneously.**

***Index Terms*—High-speed modulation, optical interconnects, semiconductor lasers, vertical-cavity surface-emitting lasers (VCSELs).**

## I. Introduction

THE vertical-cavity surface-emitting laser (VCSEL) is a suitable laser source for short-haul optical communications, owing to its ability for low-cost high-volume manufacture, low power consumption, and other unique advantages. High-speed direct modulation of a VCSEL is desired to further the transmission capacity of communication networks, such as Ethernet local area networks and board-level optical interconnects. Recently a variety of approaches have been exploited to improve the direct modulation bandwidth of VCSELs in different wavelength regimes [1]–[7]. Among the approaches taken, some enabling technologies have been identified through the optimization of VCSEL epitaxial designs, which include the tapered oxide structure [2], the buried tunnel junction [3], [7], and the incorporation of quantum-well materials with higher differential gain [2]–[6]. However, the incorporation of a photonic crystal or a generalized holey structure into the top distributed Bragg reflector (DBR) of the VCSEL offers a different optimization dimension. This approach enables us to engineer the index guiding of the transverse optical modes independent from the electrical (or current injection) aperture. A large modulation bandwidth can be achieved from reducing the optical modal volume and increasing the laser efficiency. Meanwhile, a relatively large electrical aperture can be maintained to ensure a low operation current density, enabling us to improve VCSEL reliability at the same time [8]. Moreover, the holey VCSEL approach is independent of the epitaxial design and operation wavelengths [9], and thus can be combined with other methodologies to improve modulation bandwidth.

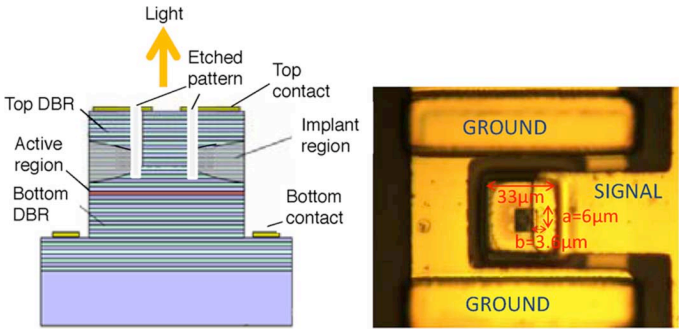


(a) (b)

Fig. 1. (a) Cross section schematic and (b) optical image of the holey VCSEL.

In our prior work, the small- and large-signal modulation characteristics of implant-confined holey VCSELs have been studied [1], [10]. Despite a maximum small-signal bandwidth (or −3-dB electrical bandwidth) of 18 GHz, the large-signal performance of holey VCSELs can be severely hindered by the carrier diffusion effect arising from the size difference between the electrical and optical apertures, making it difficult to predict the large-signal performance of a VCSEL from the small-signal measurements [10]. It was found that a small aperture size difference (less than 4 $\mu$m in diameter) can minimize the carrier diffusion effect and thus achieve large-signal modulation at higher data rates [10]. In this work, we demonstrate the 25-Gb/s operation of an implant-confined holey VCSEL with a small aperture size difference of 2.6 $\mu$m. The operation current density is as low as 7.4 KA/cm$^2$. The device design parameters, small-signal characteristics, and bit-error-ratio (BER) measurement for a multimode fiber link are also presented.

## II. Device Structure and DC Properties

Fig. 1(a) illustrates the cross section schematic of a holey VCSEL. The implant-confined VCSELs were fabricated from a wafer with a conventional 850-nm epitaxy design. Protons are implanted with 340-keV energy and a dose of $5 \times 10^{14}$ cm$^{-2}$ [11]. Coplanar ground-signal-ground contacts were deposited on planarized polyimide to reduce parasitic capacitance and facilitate on-wafer high-speed measurement. The holey structures were defined using electron beam lithography and etched approximately 16 periods (out of 21 total periods) into the top DBR. The fabrication process was discussed in more details in

Manuscript received November 02, 2009; revised December 09, 2009; accepted January 12, 2010. First published January 29, 2010; current version published March 05, 2010.

C. Chen, Z. Tian, and D. V. Plant are with Department of Electrical and Computer Engineering, McGill University, Montreal, QC H3A 2A7, Canada (e-mail: chen.chen4@mail.mcgill.ca; tianzhaobing@gmail.com; david.plant@mcgill.ca).

K. D. Choquette is with Department of Electrical and Computer Engineering, University of Illinois at Urbana-Champaign, Urbana, IL 61801 USA (e-mail: choquett@illinois.edu).

Color versions of one or more of the figures in this letter are available online at http://ieeexplore.ieee.org.

Digital Object Identifier 10.1109/LPT.2010.2040990

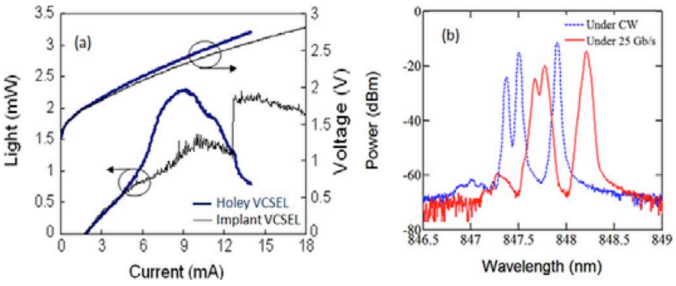


Fig. 2. (a) $L$–$I$–$V$ and (b) optical spectrum of the holey VCSEL.

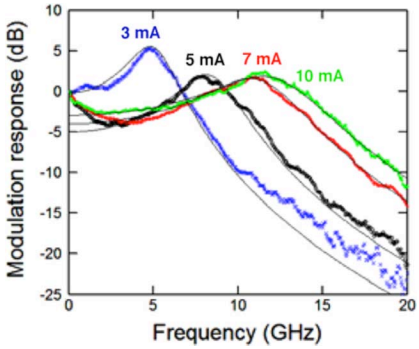


Fig. 3. Small-signal modulation characteristics of the holey VCSEL at four different dc currents.

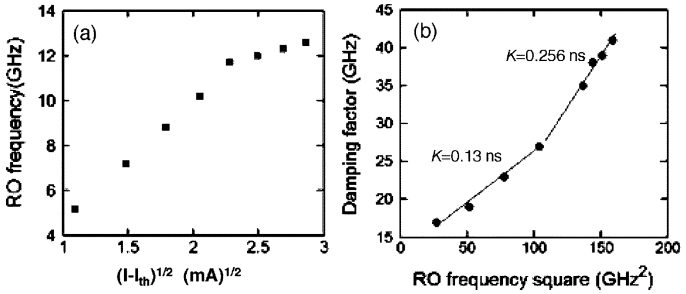


Fig. 4. (a) Measured RO frequency as a function of dc currents. (b) Damping factor as a function of RO frequency.

[1]. Fig. 1(b) shows the optical image of the holey VCSEL supporting 25-Gb/s operation reported in this work. This particular VCSEL has a 11-$\mu$m diameter implant aperture, and the lattice spacing $a = 6$ $\mu$m and hole diameter $b = 3.6$ $\mu$m, resulting in an optical aperture diameter of 8.4 $\mu$m. The aperture size difference is 2.6 $\mu$m in diameter, and thus the carrier diffusion effect is expected to diminish.

Fig. 2(a) illustrates the continuous-wave light–current–voltage ($L$–$I$–$V$) characteristics of the holey VCSEL. The holey VCSEL has a threshold current of 1.8 mA, a slope efficiency of 0.27 W/A, and a series resistance of 57.6 $\Omega$. The $L$–$I$–$V$ of an 11-$\mu$m diameter implant VCSEL without an etched pattern is also plotted for comparison. The increased slope efficiency (i.e., between 5- and 8-mA current) of the holey VCSEL is due to the decreasing diffraction loss from the improved index guiding [1]. Fig. 2(b) illustrates the optical spectrum of the holey VCESL biased at dc current of 9 mA with and without the 25-Gb/s modulation.

## III. Small- and Large-Signal Characteristics

For the high-speed modulation experiment, a lensed 50/125-$\mu$m graded-index multimode fiber (MMF) and a 25-GHz photodetector are used to collect output light from the holey VCSEL under test. For small-signal modulation, modulation voltage is supplied from a network analyzer via a 40-GHz ground–signal–ground microwave probe. For large-signal modulation, modulation voltage is supplied from a pattern generator producing a nonreturn-to-zero pseudorandom bit sequence (PRBS) of $2^7 - 1$. For a back-to-back (BTB) measurement, a 4-m 50/125-$\mu$m MMF is used; then a 100-m 50/125-$\mu$m MMF (i.e., OM2 fiber) is added to evaluate link performance over a longer distance. The eye diagrams are measured with an 80-GHz sampling oscilloscope, and BER is measured using an error detector.

Fig. 3 shows the small-signal modulation characteristics of the holey VCSEL at different dc currents. The maximum modulation bandwidth of 15.5 GHz is achieved at 10 mA. In order to obtain the laser parameters, such as the $D$-factor, the modulation current efficiency factor (MCEF) and $K$-factor, for comparison with other VCSEL technologies, the measured modulation response is fitted using the theoretical three-pole laser transfer function [12]. While the relaxation oscillation (RO) frequency is relatively easy to identify, the parasitic bandwidth is determined jointly with an equivalent circuit model through a scattering parameter $S_{11}$ measurement [13]. The calculated parasitic bandwidth is between 15 and 20 GHz for the dc current varying from 2 to 10 mA. At 10 mA, for example, the fitted junction resistance, pad capacitance, and mesa resistance (capacitance) are 32 $\Omega$, 310 fF, and 56 $\Omega$ (35 fF), respectively. In Fig. 3, the thin curves indicate the fitted responses. A large deviation from the measured responses can be seen at the frequencies below 5 GHz, consistent with our observation in the prior work [1]. This phenomenon may be attributed to the carrier diffusion from the nonuniform current density in the VCSEL transverse plane [14], or it may also be related to our present epitaxy design, for which more explanation will be given from the large-signal results.

Fig. 4(a) shows the RO frequency versus the square root of the dc current above the threshold current. The $D$-factor is 5.03 GHz/mA $^{1/2}$ measured before the RO frequency starts to saturate at the dc current of 7 mA. The MCEF is 5.57 GHz/mA$^{1/2}$ if the low frequency (<5 GHz) roll off is neglected. For a better comparison of the $D$-factor and the MEFC between the holey VCSEL and the conventional VCSEL, the aperture size difference should be considered, because the charge carriers and laser modes need to spatially overlap in order to interact effectively. For this particular holey VCSEL, if the aperture size ratio of 11 $\mu$m/8.4 $\mu$m is used, the equivalent $D$-factor and MCEF are 6.59 and 7.29 GHz/mA$^{1/2}$, respectively, which are higher than those of the 850-nm GaAs quantum-well VCSELs reported in prior work [5]. From the small-signal perspective, the equivalent $D$-factor and MCEF can be improved by reducing the optical aperture and thus the optical modal volume [12]. For a holey VCSEL, however, decreasing the optical aperture is constrained by the small aperture size difference that needs be kept in order to ensure a high data-rate large-signal operation [10]. The damping factor shows a nonlinear dependence on the square of the RO frequency, as the damping from thermal effects become more significant at higher dc currents, which makes it difficult to determine

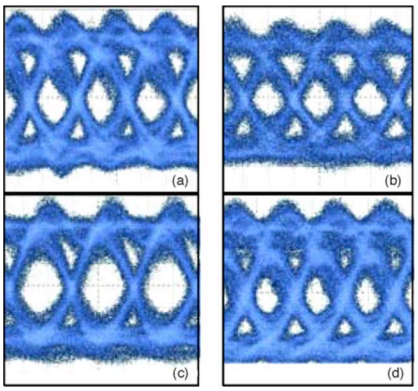


Fig. 5. Eye diagram of the holey VCSEL for (a) 25 Gb/s after BTB transmission (b) 25 Gb/s after 104-m MMF transmission (c) 20-Gb/s and (d) 28-Gb/s BTB transmission (horizontal: 20 ps/div, vertical: 0.27 mW/div).

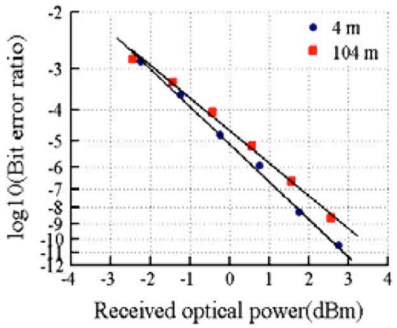


Fig. 6. BER versus received optical power after a transmission over a 4-m and 104-m MMF.

the damping limited maximum modulation bandwidth. The estimated maximum bandwidth is 34.7 GHz if the $K$-factor of 0.256 ns is used.

Fig. 5(a) and (b) illustrates the eye diagrams of the holey VCSEL at 25 Gb/s after a BTB and 104-m MMF transmission, respectively. The holey VCSEL is biased at 9 mA, and the peak–peak modulation voltage is 1 V. For the BTB (104-m MMF) transmission, the rise and fall times are 19.6 and 21.8 ps (29.3 and 28.9 ps), and the extinction ratio is 3.9 dB (3.08 dB). For comparison, Fig. 5(c) and (d) also show the eye diagrams for 20- and 28-Gb/s operation after a BTB transmission, respectively. The eye degradation is apparent at 28 Gb/s due to the limited laser bandwidth.

Fig. 6 illustrates the BER versus the received optical power after the BTB and 104-m MMF transmission at 25 Gb/s. The lowest BER for the BTB and 104-m transmission is $6.8 \times 10^{-11}$ and $2.47 \times 10^{-8}$, respectively. The power penalty results primarily from the intersymbol interference due to the MMF modal dispersion. Additionally, the BER would not be measured below $10^{-8}$, if a longer PRBS pattern (e.g., from $2^{15} - 1$ to $2^{31} - 1$) was used, which is observed for both the holey VCSEL and the implant VCSEL without an etched pattern. This may be related to the low frequency roll off observed in the small-signal experiment. Furthermore, it is important to note that, the current density of this holey VCSEL for 25-Gb/s operation is only 7.4 KA/cm$^2$ owing to its large implant aperture size. This operation current density is considerably lower than that from other high-speed VCSEL technologies [2]–[7]. Since VCSEL operation hours were found to have a power law dependence on the current density [8], a substantial improvement of VCSEL reliability should be expected.

## IV. Conclusion

In this work, we demonstrate 25-Gb/s direct modulation of an implant-confined holey VCSEL with a low current density of 7.4 KA/cm$^2$. The small-signal modulation characteristics and the BER measurements for a 100-m MMF link are also presented. With an appropriate holey structure, the size of the optical cavity can be reduced independent from that of the electrical cavity, enabling us to achieve high-speed operation and low operation current density simultaneously. This approach can be combined with other optimization methodologies or implemented at other wavelengths in the future for high-speed modulation operation.

## Acknowledgment

The authors thank P. Leisher for the fabrication of the holey VCSELs.

## References

[1] P. O. Leisher, C. Chen, J. D. Sulkin, M. S. B. Alias, K. A. M. Sharif, and K. D. Choquette, "High modulation bandwidth implant-confined photonic crystal vertical cavity surface emitting laser," *IEEE Photon. Technol. Lett.*, vol. 19, no. 19, pp. 1541–1543, Oct. 1, 2007.

[2] Y. C. Chang, C. S. Wang, and L. A. Coldren, "High-efficiency, high-speed VCSELs with 35 Gb/s error free operation," *Electron. Lett.*, vol. 43, no. 19, pp. 1022–1023, 2007.

[3] T. Anan, N. Suzuki, K. Yashiki, K. Fukatsu, H. Hatakeyama, T. Akagawa, and M. Tsuji, "High-speed 1.1-$\mu$m-range InGaAs VCSELs," in *Fiber Communication Conf.*, San Diego, CA, Mar. 2008.

[4] R. H. Johnson and D. M. Kutcha, "30 Gb/s directly modulated 850 nm datacom VCSELs," in *Conf. Lasers and Electro Optics*, San Jose, CA, May 2008.

[5] P. Westbergh, J. S. Gustavsson, A. Haglund, M. Skold, A. Joel, and A. Larsson, "High-speed, low-current-density 850 nm VCSELs," *IEEE J. Sel. Topics Quantum Electron.*, vol. 15, no. 3, pp. 694–703, May/Jun. 2009.

[6] A. Mutig, G. Fiol, K. Potschke, P. Moser, D. Arsenijevic, V. A. Shchukin, N. N. Ledentsov, S. S. Mikhrin, I. L. Krestnikov, D. A. Livshits, A. R. Kovsh, F. Hopfer, and D. Bimberg, "Temperature dependent small signal analysis of high-speed high temperature stable 980-nm VCSELs," *IEEE J. Sel. Topics Quantum Electron.*, vol. 15, no. 3, pp. 679–686, May/Jun. 2009.

[7] W. Hofmann, M. Muller, A. Nadtochiy, C. Meltzer, A. Mutig, G. Böhm, J. Rosskopf, D. Bimberg, M.-C. Amann, and C. Chang-Hasnain, "22 Gb/s long wavelength VCSELs," *Opt. Express*, vol. 17, no. 20, pp. 17547–17554, 2009.

[8] B. M. Hawkins, R. A. Hawthorne, J. K. Guenter, J. A. Tatum, and J. R. Biard, "Reliability of various size oxide aperture VCSELs," in *Electronic Components and Technology Conf.*, San Diego, CA, 2002.

[9] A. M. Kasten, M. P. Tan, J. D. Sulkin, P. O. Leisher, and K. D. Choquette, "Photonic crystal vertical cavity lasers with wavelength independent single mode behavior," *IEEE Photon. Technol. Lett.*, vol. 20, no. 23, pp. 2010–2012, Dec. 1, 2008.

[10] C. Chen, P. O. Leisher, D. M. Kuchta, and K. D. Choquette, "High-speed modulation of index-guided implant-confined vertical cavity surface emitting lasers," *IEEE J. Sel. Topics Quantum Electron.*, vol. 15, no. 3, pp. 673–678, May/Jun. 2009.

[11] K. D. Choquette and K. M. Geib, "Fabrication and performance of vertical-cavity surface-emitting lasers," in *Vertical-Cavity Surface-Emitting Lasers*, C. W. Wilmsen, H. Temkin, and L. A. Coldren, Eds. New York: Cambridge Univ. Press, 1999, pp. 193–232.

[12] L. A. Coldren and S. W. Corzine, *Diode Lasers and Photonic Integrated Circuits*. New York: Wiley, 1995.

[13] A. N. AL-Omari and K. L. Lear, "Polyimide planarized vertical-cavity surface-emitting lasers with 17.0-GHz bandwidth," *IEEE Photon. Technol. Lett.*, vol. 16, no. 4, pp. 969–971, Apr. 2004.

[14] R. S. Tucker and D. J. Pope, "Circuit modeling of the effect of diffusion on damping in a narrow-strip semiconductor laser," *IEEE J. Quantum Electron.*, vol. 19, no. 7, pp. 1179–1183, Jul. 1983.